



Crack bridging in ceramic-based nanocomposites reinforced with hybrid graphene/alumina nanofibers

S.V. Bobylev ¹ ✉, A.G. Sheinerman ²

¹ Peter the Great St. Petersburg Polytechnic University, St. Petersburg, Russia

² Institute for Problems of Mechanical Engineering RAS, St. Petersburg, Russian Federation

✉ bobylev.s@gmail.com

Abstract. A model is proposed describing the effect of crack bridging on the fracture toughness of ceramic-based nanocomposites reinforced with hybrid graphene/alumina nanofibers. Within the model, a mode I crack propagates normally to a system of aligned inclusions, whose pullout from the ceramic matrix in the wake of the crack toughens the composite. The dependences of the fracture toughness on the graphene content and the sizes of the inclusions are calculated in the exemplary case of yttria stabilized zirconia based composites. The calculations predict that if crack bridging is the dominant mechanism during crack growth, the maximum toughening can be achieved in the case of long nanofibers provided that the latter do not rupture and adhere well to the matrix. The model shows good correlation with the experimental data at low graphene concentrations.

Keywords: fracture toughness, crack bridging, graphene, nanofibers, yttria stabilized zirconia

Acknowledgements. This work was supported by the Russian Science Foundation (grant 18-19-00255).

Citation: Bobylev SV, Sheinerman AG. Crack bridging in ceramic-based nanocomposites reinforced with hybrid graphene/alumina nanofibers. *Materials Physics and Mechanics*. 2023;51(3): 1-8. DOI: 10.18149/MPM.5132023_1.

Introduction

Structural ceramic materials are an actively developed field of research for advanced engineering applications due to their excellent properties such as high strength, chemical inertness, high temperature stability, and good wear performance [1–5]. However, monolithic ceramics tend to be mechanically unreliable, which limits their use in applications where damage tolerance is a main requirement [6–9]. Therefore, a wide range of reinforcing and/or toughening agents have been incorporated into ceramic matrices in attempt to produce tough ceramic-matrix composites [9–12]. Due to their superior mechanical, optical and thermal properties, high electrical conductivity and a large specific surface area, nanosized allotropes of carbon, such as carbon nanotubes (CNT) and graphene nanoplatelets (GNPs), are excellent nanofillers in ceramic-matrix composites [9–12].

For example, the incorporation of either CNTs or GNPs into ceramic-matrix composites has been shown to significantly improve fracture toughness and flexural strength [8,9,13]. The authors of Ref. [9] found an increase in the fracture toughness of silicon nitride by 135 percent by adding 1.5 volume percent of GNPs. Such a dramatic increase in fracture toughness was explained [14] primarily by the formation of dense ensembles of graphene sheets that surround individual grains and cause a change in the direction of growing cracks. Lee et al. [15] observed

a 2.5-fold increase of the fracture toughness of alumina after the addition of 2 vol. % of reduced graphene oxide. Another example of a significant increase in fracture toughness is tantalum carbide [16], in which GNPs increased the fracture toughness by 99 percent. At the same time, many similar studies of ceramics toughened by GNPs have not demonstrated such strong toughening.

Recently, the novel type of hybrid nanofillers representing alumina (Al_2O_3) nanofibers of several nanometres in diameter encapsulated with multi-layered graphene shells have been introduced [17–19]. Experimental studies [17–19] demonstrated that the presence of these nanofillers results in simultaneous improvement in indentation fracture toughness and hardness, as well as significantly improved electrical properties.

Electron microscopy observations (see, e.g., reviews [6,20–22]) of cracks and fracture surfaces of ceramic/graphene composites highlight a very important role of crack bridging combined with inclusions pull-out in the toughening of ceramic/graphene composites. The important role of crack bridging is further supported by the character of crack resistance curves [20] (which demonstrate a significant increase of the fracture toughness with the crack length). Therefore, in the following, we will employ the method developed in our previous works [23,24] for the description of the effect of crack bridging in ceramic composites reinforced with hybrid graphene/alumina nanofibers on their fracture toughness, depending on the volume fraction and geometric parameters of inclusions.

Model of crack bridging in ceramic nanocomposite reinforced with hybrid graphene/alumina fibers

Let us consider crack propagation in a deformed composite specimen reinforced with inclusions in a form of hybrid graphene/alumina nanofibers (nanofibers in a shell of multilayer graphene; see Fig. 1). To do so, we use the approach developed in our earlier works [23,24]. In the framework of this approach, we consider a model straight semi-infinite mode I crack intersecting a system of identical inclusions (with the equal length l and radius r) perpendicular to the crack plane (Fig. 2). In the region behind the crack tip where the distance between the crack surfaces is smaller than the inclusion length l , referred to as the crack-bridging zone, inclusions form bridges between crack surfaces. The friction between the inclusions and the ceramic matrix produces the bridging forces, acting at each matrix/inclusion interface (Fig. 2). These forces create a resistance to the crack opening, thereby increasing fracture toughness of the composite.

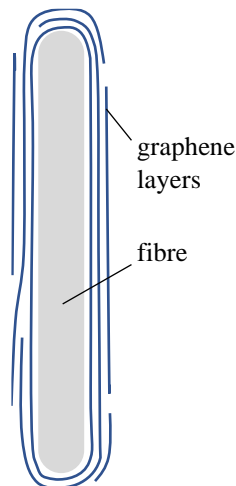


Fig. 1. Schematic representation of hybrid nanofiber

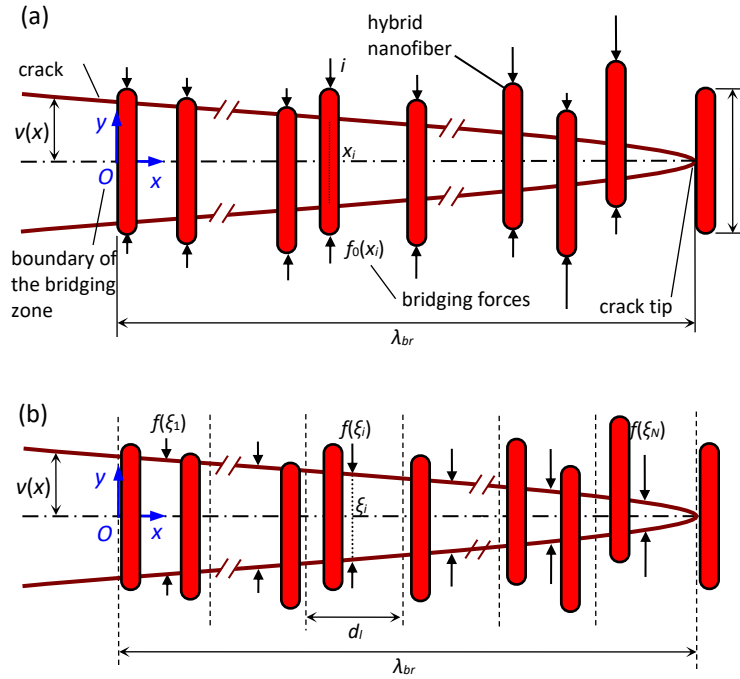


Fig. 2. (a) Crack in a ceramic composite reinforced with aligned hybrid nanofibers. The traction in the crack-bridging zone is discretized into a series of concentrated forces $f(x_i)$. (b) Illustration of calculation scheme. Crack bridging zone is divided into a system of identical layers with width d_i . Each layer produces integral bridging force $f(\xi_i)$

Following the approach of the model [24] we assume that centers of inclusions are arranged randomly relative to the crack plane. Consequently, the friction forces are different at upper and lower crack surfaces. However, the pullout process is controlled by a smaller force (at the side where the inclusion immersion depth into the matrix is smaller). It is obvious that the initial depth of immersion may vary from 0 to $l/2$. In order to account for the random arrangement of inclusions, we assume that the initial depth of their immersion into the matrix is equal to the mean immersion depth, i.e., $l/4$. Friction forces are distributed along cylindrical lateral surfaces of inclusions, but it is convenient to replace them with the equivalent concentrated loads applied along inclusion axes (Fig. 2(a)). Then, in a Cartesian coordinate system (x, y) , with the origin at the bridging zone boundary (Fig. 2) the friction forces at the matrix/inclusion interface boundaries are written as follows [24]:

$$f_0(x_i) = 2\pi\tau(x_i)r\left[\frac{l}{4} - v(x_i)\right]. \quad (1)$$

Here x_i are the coordinates of the inclusions (their centers) (i takes the integers from 1 to n , where n is the total number of inclusions in the crack-bridging zone), $v(x_i)$ is the crack opening displacement at the position $x = x_i$ (which is equal to the pull-out length of the platelet at the same location), $\tau(x_i)$ is the average shear stress at the interface between the bridging platelet and the matrix. In the following, we assume that the stress $\tau(x_i)$ does not depend on the crack opening displacement at the point $x = x_i$ and put $\tau(x_i) = \tau_0$, where τ_0 is a material constant.

Since inclusions are randomly distributed in the material, we do not know their coordinates, and therefore cannot directly determine the forces f_0 . Nevertheless, we can describe these forces with the help of the following procedure developed in works [23,24]. We divide

the crack-bridging zone into a system of N identical layers whose width d_l in the crack growth direction is small compared to the length λ_{br} of the crack bridging zone (see Fig. 2(b)). In this case, the crack opening displacements v can be considered constant within each layer. We approximate an ensemble of the concentrated forces acting within each layer at the matrix/inclusion interfaces by a single concentrated force $F(\xi_i)$ defined as the sum of the forces created by all the inclusions contained within this layer. We also assume that the forces $F(\xi_i)$ act in the middle section of each layer at the positions given by the coordinates (in the coordinate system shown in Fig. 2(b))

$$\xi_i = (i-1/2)d_l, \quad i = 1, 2, \dots, N. \quad (2)$$

The forces $F(\xi_i)$ can be expressed as

$$F(\xi_i) = 2\pi\tau_0 r \left[\frac{l}{4} - v(x_i) \right] N_{gr}. \quad (3)$$

Here the factor $2\pi\tau_0 r [l/4 - v(\xi_i)]$ represents the force, given by formula (1), N_{gr} is the average number of inclusions within one layer. If we assume uniform distribution of inclusions within composite, then N_{gr} is the same in all layers and can be estimated as follows. If the crack width (in the direction normal to Fig. 2 plane) is W then all inclusions intersecting the crack plane are contained within a parallelepiped with dimensions $2l \times d_l \times W$ and volume $V = 2ld_lW$. The total volume of graphene V_{gr} inside this parallelepiped is equal $V_{gr} = N_{gr}V_0 = N_{gr}2\pi r l h$, where $V_0 = 2\pi r l h$ is the volume of single graphene shell covering the inclusion (h is graphene shell thickness). Volume fraction c of graphene by definition $c = V_{gr} / V = N_{gr}\pi r h / (d_l W)$. From here we find

$$N_{gr} = \frac{2cd_lW}{\pi r h}. \quad (4)$$

From Eqs. (3) and (4) we derive force $F(\xi_i)$:

$$F(\xi_i) = \frac{cd_lW}{2h} \tau_0 [l - 4v(\xi_i)]. \quad (5)$$

And force the forces per unit length of the layers in the direction of the z -axis (see Fig. 2b) are given as

$$f(\xi_i) = F(\xi_i) / W = \frac{cd_l}{2h} \tau_0 [l - 4v(\xi_i)]. \quad (6)$$

These forces are exactly half in magnitude compared to forces in case of composites reinforced with flat graphene nanoplatelets [23,24] which is expected because in present case graphene sheets contact with matrix by one side only instead of both.

The fracture toughness K_{IC} of the composite can be written [23–25] as

$$K_{IC} = K_I^0 - K_I^{br}, \quad (7)$$

where K_I^0 is the fracture toughness without the toughening effect of crack-bridging inclusions and K_I^{br} is the total stress intensity factor created by the bridging forces, which is negative. The stress intensity factor K_I^{br} is expressed [23–25] as

$$K_{IC} = K_I^0 - \sqrt{\frac{2}{\pi}} \frac{cd_l\tau_0}{2h} \sum_{i=1}^N \frac{l - 4v(\xi_i)}{\sqrt{\lambda_{br} - \xi_i}}. \quad (8)$$

The absolute value of K_I^{br} increases with increasing λ_{br} , eventually reaching saturation when the crack enters the steady-state propagation mode [25], in which the crack propagates

but the crack-bridging zone is kept at a constant length. In the steady-state mode, a new platelet bridge formed at the right end of the crack-bridging zone is always accompanied by a complete pull-out of a platelet at the left end.

In order to use formula (8), one should calculate the crack opening displacements $v(\xi_i)$. This is achieved by solving the following system on N linear equations [23–25]:

$$v(\xi_i) = \frac{4K_I^0 \sqrt{\lambda_{br} - \xi_i}}{\sqrt{2\pi E}} + \frac{cd_1\tau_0 \sqrt{\lambda_{br} - \xi_i}}{\pi Eh} \sum_{n=1}^N \frac{l - 4v(\xi_n)}{\sqrt{\lambda_{br} - \xi_n}} - \frac{cd_1\tau_0}{2\pi Eh} p.v. \sum_{n=1}^N [l - 4v(\xi_n)] \ln \frac{\sqrt{\lambda_{br} - \xi_i} + \sqrt{\lambda_{br} - \xi_n}}{\left| \sqrt{\lambda_{br} - \xi_i} - \sqrt{\lambda_{br} - \xi_n} \right|}. \quad (9)$$

Here, E is the Young's modulus and $p.v.$ stands for discrete Cauchy principal value (the definition and the instructions on how to calculate $p.v.$ can be found in the Appendix of Ref. [20]). The length of the bridging zone appearing in formula (9) is defined as $\lambda_{br} = Nd_1$. For definiteness, we also initially put $d_1 = 3l$, in which case the relation $d_1 \ll \lambda_{br}$ should be satisfied, as a rule. (In the latter case K_{IC} should not depend on d_1 .) To calculate the number N of the layers, we solve the system of linear equations (9) for various N until the relation $v(\xi_1) \approx l/4$ is satisfied (we find the value of N that gives $v(\xi_1)$ as close to $l/4$ as possible). If for the calculated value of N , the relation $d_1 \ll \lambda_{br}$ is not fulfilled, we decrease the value of d_1 and repeat the calculations. If the solution of system (9) gives $v(\xi_i) < 0$ in a small region very close to the crack tip, we put $v(\xi_i) = 0$ in this region. After solving equations (9), for specified values of K_I^0 and τ_0 , we can calculate the fracture toughness K_{IC} of the composite using formulae (7) and (8).

Results and discussion

In this section, we calculate the dependences of the fracture toughness of ceramic/graphene composites on various parameters in the exemplary case of yttria stabilized zirconia (YSZ)-based composite reinforced with hybrid alumina fibers using the experimental data from Ref. [19]. All the calculations are performed for the steady-state crack propagation mode characterized by sufficiently large crack lengths (see the previous section). We calibrated our model using experimental data [19] for the case of low graphene contents (when fracture toughness is not expected to decay due to increasing porosity, typical of the ceramic/graphene composites with a high graphene concentration). For the YSZ specimens with characteristic fibers dimensions $l = 1 \mu\text{m}$ and $r = 7 \text{ nm}$, experimental results [19] are as follows: $K_I^0 = 5.73 \text{ MPa}\cdot\text{m}^{1/2}$; $\eta = K_{IC} / K_I^0 = 1.09$ for $c = 0.2 \text{ vol.}\%$ and $\eta = 1.21$ for $c = 0.6 \text{ vol.}\%$.

Using the value of the Young modulus $E = 577 \text{ GPa}$ for unreinforced YSZ [26] and the values of other parameters specified above, we obtained good fit to experimental data [19] at $\tau_0 = 370 \text{ MPa}$. In this case, our calculations give: $\eta \approx 1.08$ and 1.22 for $c = 0.2$ and $0.6 \text{ vol.}\%$, respectively. At high graphene concentrations, however, the calculated toughening ratio $\eta = K_{IC} / K_I^0$ considerably exceeds the experimental values, which can be attributed to an increase in porosity or the activation of other mechanisms reducing fracture toughness. For example, for $c = 1 \text{ vol.}\%$ our model gives, $\eta \approx 1.33$ whereas the measured fracture toughness is about the same as that of unreinforced YSZ ($\eta \approx 1.01$).

Now we can plot the dependences of the toughening ratio $\eta = K_{IC} / K_I^0$ on various parameters (c , l) to obtain theoretical estimates for the crack-bridging induced toughening.

Below we put $\tau_0 = 370$ MPa, $E = 577$ GPa [26] and $K_I^0 = 5.73$ MPa·m^{1/2} [19]. Figure 3 shows the dependences of the toughening ratio η on the graphene volume fraction c for various values of the inclusion length l (Fig. 3(a)). The curves in Fig. 3(a) are calculated for $h = 2.5$ nm and $r = 3.5$ nm. Figure 3 demonstrates that the toughening ratio η increases with increasing the graphene content c in the composite, and the normalized increase in fracture toughness due to graphene $(K_{IC} - K_I^0) / K_I^0 = \eta - 1$ scales with the graphene volume fraction c approximately as $\eta - 1 \sim c^{0.8}$.

Figure 3(b) shows the dependences of the toughening ratio η on the nanofiber length l for various values of the graphene volume fraction c . Figure 3(b) demonstrates that the toughening ratio η increases with increasing platelet length. Although for a fixed graphene volume fraction c , a higher platelet length means fewer inclusions in the composite, the fact that a longer inclusion is much harder to pull out from the matrix due to a larger area of the interface between the inclusion and the matrix easily beats the former factor.

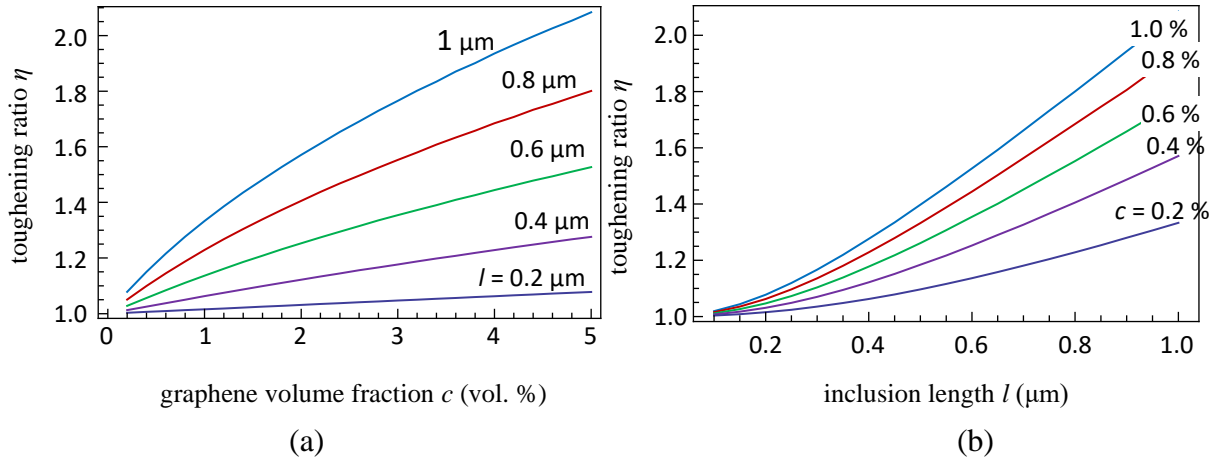


Fig. 3. Dependences of the toughening ratio η of YSZ-matrix composite reinforced with graphenized alumina nanofibers on (a) the graphene volume fraction c and graphene shell thickness $h = 2.5$ nm and various values of the nanofiber length l ; (b) the nanofiber length l and various values of graphene volume fraction c

Figure 3 demonstrate that if crack bridging is the dominant mechanism controlling crack propagation in YSZ/graphene composites, it can increase fracture toughness by up to $\sim 100\%$, depending on the amount of graphene in the composite and platelet dimensions. This toughness improvement is comparable with the typical experimentally observed toughening values for hybrid nanofibers, CNTs and GNPs [19,27,29] (usually about 20–60 %).

Concluding remarks

Thus, we have suggested a model describing the effect of crack bridging on the fracture toughness of ceramic nanocomposite reinforced with graphenized alumina nanofibers (hybrid nanofibers with alumina core wrapped in a shell of multilayer graphene). Within the model, a mode I crack propagates normally to a system of aligned inclusions, whose pullout from the ceramic matrix in the wake of the crack toughens the composite. For the exemplary case of YSZ-matrix composite reinforced with graphenized alumina nanofibers, we have demonstrated that the crack-bridging-induced fracture toughness enhancement $K_{IC} - K_I^0$ scales with the graphene volume fraction c approximately as $K_{IC} - K_I^0 \sim c^{0.8}$. The calculations also revealed that, for a specified graphene volume fraction, longer fibers produce better crack-bridging-

related toughening than smaller ones.

At the same time, for a specified volume fraction of graphene, large inclusions are characterized by higher average spacing, which can result in a less uniform distribution and thereby reduce the fracture toughness of the composite. In addition, if the inclusions do not adhere very well to the matrix, long inclusions produce weak interfaces that can themselves initiate fracture or promote the propagation of existing cracks. For example, in alumina/graphene composites, an increase in the length of GNPs can activate sliding over the alumina/graphene interfaces near crack tips, which was shown to reduce fracture toughness [29]. Thus, the structural design of tough ceramic/graphene composites requires a simultaneous account for multiple crack propagation mechanisms. This will be the subject of the further investigations of the authors.

References

1. Xiang H, Xing Y, Dai F, Wang H, Su L, Miao L, Zhang G, Wang Y, Qi X, Yao L, Wang H, Zhao B. High-entropy ceramics: Present status, challenges, and a look forward. *J. Adv. Ceram.* 2021;10(3): 385–441.
2. Fattahi M, Babapoor A, Delbari SA, Ahmadi Z, Sabahi Namini A, Shahedi Asl M. Strength-ening of TiC ceramics sintered by spark plasma via nano-graphite addition. *Ceram. Int.* 2020;46(8): 12400–12408.
3. Ni D, Cheng Y, Zhang J, Liu J-X, Zou J, Chen B, Wu H, Li H, Dong S, Han J, Zhang X, Fu Q. Advances in ultra-high temperature ceramics, composites, and coatings. *J. Adv. Ceram.* 2022;11(1): 1–56.
4. Liu Y, Jiang X, Shi J, Luo Y, Tang Y, Wu Q, Luo Z. Research on the interface properties and strengthening-toughening mechanism of nanocarbon-toughened ceramic matrix composites. *Nanotechnol. Rev.* 2020;9(1): 190–208.
5. Wei ZY, Meng GH, Chen L, Li GR, Liu MJ, Zhang WX, Zhao LN, Zhang Q, Zhang XD, Wan CL, Qu ZX, Chen L. Progress in ceramic materials and structure design toward ad-vanced thermal barrier coatings. *J. Adv. Ceram.* 2022;11(7): 985–1068.
6. Porwal H, Grasso S, Reece MJ. Review of graphene–ceramic matrix composites. *Adv. Appl. Ceram.* 2013;112: 443–454.
7. Grasso S, Yoshida H, Porwal H, Sakka Y, Reece M. Highly transparent α -alumina obtained by low cost high pressure SPS. *Ceram. Int.* 2013;39: 3243–3248.
8. Belghalem H, Hamidouche M, Gremillard L, Bonnefont G, Fantozzi G. Thermal shock resistance of two micro-structured alumina obtained by natural sintering and SPS. *Ceram. Int.* 2014;40: 619–627.
9. Liu J, Yan H, Jiang K. Mechanical properties of graphene platelet-reinforced alumina ceramic composites. *Ceram. Int.* 2013;39: 6215–6221.
10. Drozdova M, Hussainova I, Pérez-Coll D, Aghayan M, Ivanov R, Rodríguez MA. A novel approach to electroconductive ceramics filled by graphene covered nanofibers. *Mater. Des.* 2016;90: 291–298.
11. Porwal H, Tatarko P, Grasso S, Khaliq J, Dlouhý I, Reece MJ. Graphene reinforced alumina nanocomposites. *Carbon.* 2013;64: 359–369.
12. Berdova M, Pyymaki Perros A, Kim W, Riikonen J, Ylitalo T, Heino J, Li C, Kassamakov I, Hæggröm E, Lipsanen H, Franssila S. Corrigendum: exceptionally strong and robust millimeterscale graphene–alumina composite. *Nanotechnology.* 2014;25: 439501.
13. Fan Y, Kang L, Zhou W, Jiang W, Wang L, Kawasaki A. Control of doping by matrix in few-layer graphene/metal oxide composites with highly enhanced electrical conductivity. *Carbon.* 2015;81: 83–90.
14. Walker LS, Marroto VR, Rafiee MA, Koratkar N, Corral EL. Toughening in graphene ceramic composites. *ACS Nano.* 2011;5: 3182–3190.

15. Lee B, Koo MY, Jin SH, Kim KT, Hong SH. Simultaneous strengthening and toughening of reduced graphene oxide/alumina composites fabricated by molecular-level mixing process. *Carbon*. 2014;78: 212–219.
16. Nieto A, Lahiri D, Agarwal A. Graphene NanoPlatelets reinforced tantalum carbide consolidated by spark plasma sintering. *Mater. Sci. Eng. A*. 2013;582: 338–346.
17. Drozdova M, Pérez-Coll D, Aghayan M, Ivanov R, Rodríguez MA, Hussainova I. Hybrid graphene/alumina nanofibers for electroconductive zirconia. *Key Eng. Mater.* 2016;674: 15–20.
18. Hussainova I, Baronins J, Drozdova M, Antonov M. Wear performance of hierarchically structured alumina reinforced by hybrid graphene encapsulated alumina nanofibers. *Wear*. 2016;368-369: 287–295.
19. Hussainova I, Drozdova M, Pérez-Coll D, Rubio-Marcos F, Jasiuk I, Soares J.A.N.T., Rodríguez MA. Electroconductive composite of zirconia and hybrid graphene/alumina nanofibers. *J. Eur. Ceram. Soc.* 2017;37: 3713–3719.
20. Centeno A, Rocha VG, Alonso B, Fernandez A, Gutierrez-Gonzalez CF, Torrecillas R, Zurutuza A. Graphene for tough and electroconductive alumina ceramics. *J. Eur. Ceram. Soc.* 2013;33(15-16): 3201–3210.
21. Nieto A, Bisht A, Lahiri D, Zhang C, Agarwal A. Graphene reinforced metal and ceramic matrix composites: a review. *Int. Mater. Rev.* 2017;62: 241.
22. Miranzo P, Belmonte M, Osendi MI. From bulk to cellular structures: A review on ceramic/graphene filler composites. *J. Eur. Ceram. Soc.* 2017;37(2): 3649–3672.
23. Bobylev SV, Sheinerman AG. Effect of crack bridging on the toughening of ceramic/graphene composites. *Rev. Adv. Mater. Sci.* 2018;57: 54–62.
24. Bobylev SV. Effect of graphene platelets pullout from ceramic matrix on the fracture toughness of ceramic/graphene composites. *Phys. Solid State*. 2022;6: 677.
25. Shao Y, Zhao HP, Feng XQ, Gao H. Discontinuous crack-bridging model for fracture toughness analysis of nacre. *J. Mech. Phys. Solids*. 2012;60(8): 1400–1419.
26. Muhammad ID, Awang M, Mamat O. Modelling the elastic constants of cubic zirconia using molecular dynamics simulations. *Adv. Mater. Res.* 2014;845: 387.
27. Shin JH, Hong SH. Fabrication and properties of reduced graphene oxide reinforced yttria-stabilized zirconia composite ceramics. *J. Eur. Ceram. Soc.* 2014;34: 1297–1302.
28. Liu J, Guo H, Su Y, Wang L, Wei L, Yang G, Yang Y, Jiang K. Spark plasma sintering of graphene platelet reinforced zirconia composites with improved mechanical performance. *Mater. Sci. Eng. A*. 2017;688: 70–75.
29. Porwal H, Saggarr R, Tatarko P, Grasso S, Saunders T, Dlouhý I, Reece MJ. Effect of lateral size of graphene nano-sheets on the mechanical properties and machinability of alumina nanocomposites. *Ceram. Int.* 2016;42(6): 7533–7542.

THE AUTHORS

Bobylev S.V. 

e-mail: bobylev.s@gmail.com

Sheinerman A.G. 

e-mail: asheinerman@gmail.com